

**AAE 520**  
**Experimental Aerodynamics**  
**Professor Schneider**

**Experiment 1:**  
**Hot Wires, Wakes, and Drag Measurement**

Purdue University  
School of Aeronautics and Astronautics

Performed by: Micah Chibana and Edward Kay

2/9/2004

# Hot Wires, Wakes, and Drag Measurement

## 1. Abstract

Using a subsonic wind tunnel, the wake of a cylinder and a NACA 0010 airfoil were investigated using hot wire measurements of the air velocity downstream from the objects. Integrating the profile of the velocity across the wake perpendicular to the flow gives a measurement of the drag on the bodies. This technique was used to evaluate drag at various velocities and at various positions downstream from the objects. The airfoil was also studied at an angle of attack. In the performance of this lab we were able to gain experience using hot wires and the related experimental equipment, while at the same time obtaining experimental measurements of the drag coefficient,  $C_d$ , that were in agreement with theoretical values. Other measurements confirmed that the cylinder wake remains self-similar as it travels downstream.

## 2. Introduction

Whenever an object is moving in a fluid (or whenever a fluid is moving relative to an object) at a large enough speed ( $Re > 1$ ), there is always a wake trailing behind. This is easily seen in the trailing wake behind boats as they drive through water. Often the fluid flowing in this wake is turbulent and hard to predict without the use of experimental techniques. Studying the velocities of the fluid in this wake can give a measurement of the drag on the object. For most applications such as airplanes, boats, and cars the design of the object's shape is critical in reducing the drag on the object, thus creating a better performing vehicle. Fluid mechanics gives a formulation of the physics behind fluid flow and has largely studied the flow around cylinders. This forms the motivation behind our study of cylinder wakes, due to the ease of comparison to theoretical predictions. Measuring the wake of an airfoil should give a nice comparison/contrast to the cylinder, giving a real world application to this experiment.<sup>1</sup>

## 2.1 Objectives

The objectives of the experiment were to:

- Observe the structure of a wake.
- Use velocity profile information to calculate the drag on a body.
- Become familiar with using a hot-wire anemometer.
- Compare the results from various cylinder and airfoil wakes, under downstream conditions.

## 3. Background

### 3.1 Pitot-Static Tube

When studying the flow for an inviscid, incompressible fluid of density  $\rho$  along a streamline, Bernoulli's equation gives a relation between the static pressure ( $P_s$ ), total pressure ( $P_t$ ), and the average velocity of the flow ( $U$ ).<sup>2</sup>

$$P_s + \frac{1}{2}\rho U^2 = P_t \quad (1)$$

A pitot-static tube uses a pitot tube for measuring the total pressure and a static tube to obtain a measurement of the static pressure (Fig.1). Once these two quantities are measured equation 1 can be rewritten to obtain the value for the velocity of the fluid.<sup>1</sup>

$$U = \sqrt{\frac{2(P_t - P_s)}{\rho}} \quad (2)$$

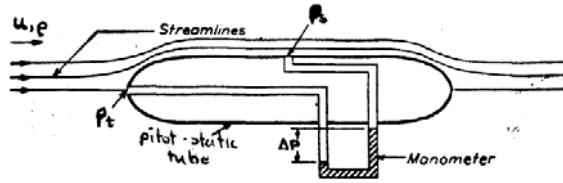


Figure 1: A pitot-static tube is aligned along a streamline to give a measurement of  $\Delta P$ .<sup>1</sup>

### 3.2 Hot Wire Sensor

Another tool used in the measurement of fluid velocity is the hot wire sensor (Fig. 2). A hot wire consists of a thin thread of wire placed perpendicular to the flow that is heated and kept at a constant temperature by an anemometer. When the wire is placed in the flow, the passing fluid cools the wire. Since the anemometer is keeping the wire at a constant temperature, the voltage passing through the wire must increase when fluid is passing. Thus, the anemometer measures the amount of heat transferred to the fluid from the wire.

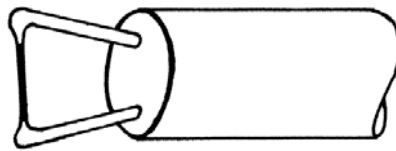


Figure 2: Hot wire sensor<sup>1</sup>

King's Law gives an empirical formula relating the voltage applied to the wire ( $V$ ) and the velocity of the fluid ( $U$ ).

$$\sqrt{U} = AV^2 + B \quad (3)$$

### 3.3 Cylinder Wake: Laminar and Turbulent Flow

Flow around a cylinder has been a thoroughly studied topic in fluid mechanics. Figure 3 shows a variety of flow patterns as the velocity of the fluid is increased. The Reynolds

number gives an indication on the velocity of the fluid flow for a given sized object ( $d$ ), where  $\nu$  is the kinematic viscosity of the fluid.

$$Re = (U*d)/\nu \quad (4)$$

When the fluid is moving at Reynolds numbers less than one, there is no wake and the streamlines are symmetrical (Fig. 3A).

When the Reynolds number is increased above one, the streamlines no longer close directly around the back of the cylinder.

Instead, they create a pair of stationary (Floppl) vortices that close downstream (Fig. 3B).

With even greater  $R$ , the vortices elongate (Fig. 3C) and eventually detach (for  $R > 40$ ) in a shedding pattern (Figs. 3D and 3E). This is known as von Karman vortex shedding. Its frequency ( $f$ ) is related to the Strouhal number,  $S$ , by the diameter of the cylinder ( $d$ ) and the free stream velocity ( $U_\infty$ ). An empirical curve relating the Strouhal number to the Reynolds number is given in the appendix (Fig 15).<sup>3</sup>

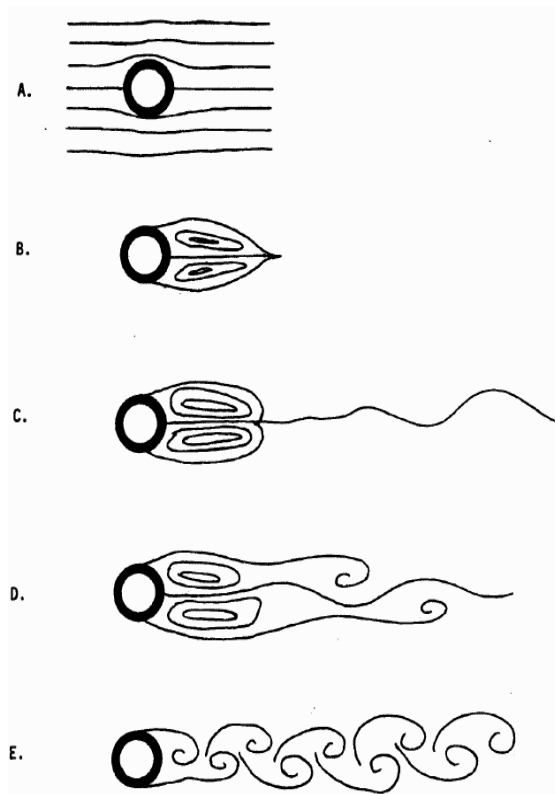


Figure 3: Flow behind a cylinder. Flow is from left to right.<sup>3</sup>

$$S = (d*f)/U_\infty \quad (5)$$

The two characteristic types of fluid flow are laminar and turbulent. Fluid particles in a laminar flow follow smooth trajectories without much mixing between layers of the fluid. Turbulent flow is more chaotic as particle movement is seemingly random with layers of the fluid mixing in complex patterns. While turbulent flow is hard to predict, it is much more common than laminar flow and often must be analyzed using experimental measurements. In the wake of a cylinder, the flow is often turbulent and the velocity is

lower than in the free stream. Figure 4 shows the turbulent wake behind a cylinder and the profile of the velocity deficit in the wake.

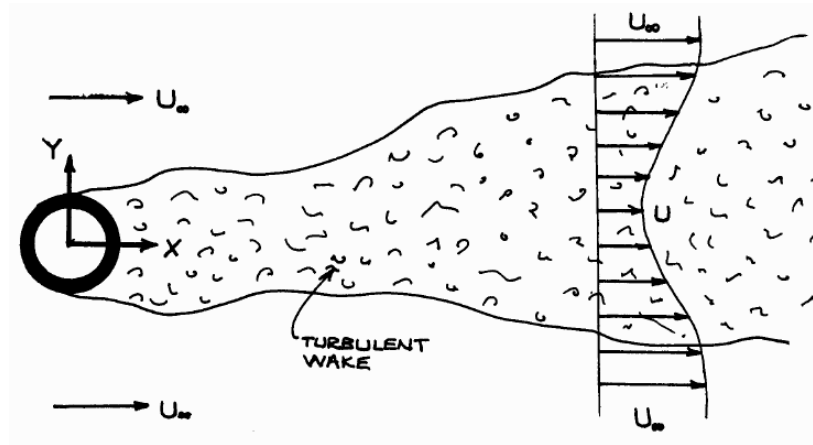


Figure 4: Turbulent wake and velocity profile behind a cylinder<sup>3</sup>

This deficit can be viewed as energy lost from the free stream and integrating it across the wake can give a measure of the total drag force acting on a body. Given the velocity profile components (Fig. 5), the velocity deficit ( $u_1$ ) can be written as:

$$u_1 = U_\infty - u \quad (6)$$

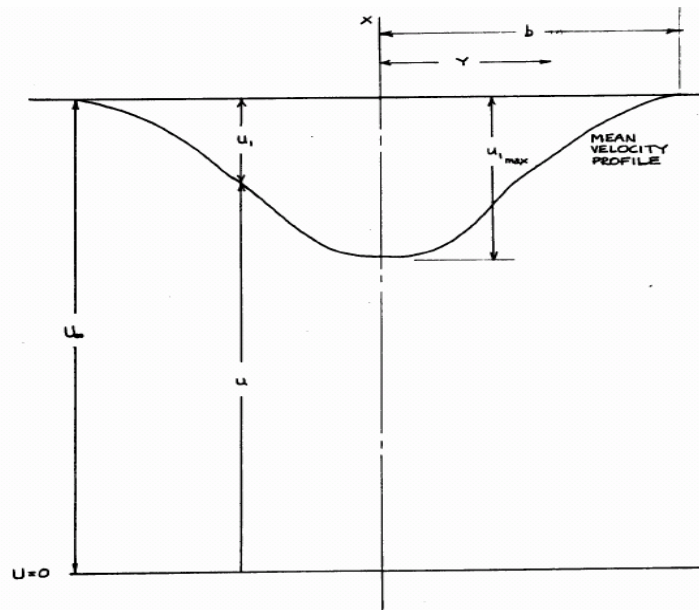


Figure 5: Geometry of the velocity profile in a wake<sup>3</sup>

Moving away from the wake  $u$  converges to  $U_\infty$ . The total drag ( $D$ ) is found by considering the conservation of momentum in a control volume enclosing the cylinder.

$$D = h\rho \int_{-\infty}^{+\infty} u(U_\infty - u)dy \quad (7)$$

$$D = h\rho \int_{-\infty}^{+\infty} u_1(U_\infty - u_1)dy \quad (8)$$

Here Eqn. 6 has been used to put Eqn. 7 in terms of the height of the body ( $h$ ), velocity deficit at point  $y$  ( $u_1$ ), and the fluid density ( $\rho$ ). Another to express the drag force ( $D$ ) is in terms of the frontal area of the body ( $A$ ) and the drag coefficient ( $C_d$ ).

$$D = \frac{1}{2}\rho AU_\infty^2 C_d \quad (9)$$

An empirical curve fit for the  $C_d$  of a cylinder is:

$$C_d \approx 1 + 10.0R^{-2/3} \quad (10)$$

Another result from fluid mechanics is that as the velocity is observed downstream from the cylinder the profile should remain self-similar in shape.

$$\frac{u_1}{u_{1\max}} = [1 - (y/b)^{3/2}]^2 \quad (11)$$

Thus, the curve shape should be independent of the downstream location given  $x/(C_d*d) > 50$ . This self-similarity of the profile and the empirical curve for  $C_d$  will be compared to results found in this lab.<sup>3</sup>

## 4. Procedure

### 4.1 Tunnel Setup

The diagram of the experimental setup is shown in figure 6, consisting of the subsonic wind tunnel, pitot tube, manometer, hot wire, transversing mechanism, anemometer, oscilloscope, and Fluke 77. The pitot tube is connected to the manometer for pressure measurements as described in section 3.1. Downstream in the flow from the object being studied is the hot wire which sits on a transversing mechanism. This allows the location of the hot wire to be adjusted perpendicular to the free stream flow. A micrometer on the mechanism allows for accurate position measurements. The anemometer keeps the hot wire at a constant temperature while its output shows the voltage applied to the hot wire on the oscilloscope display. The Fluke is also there for voltage measurements.

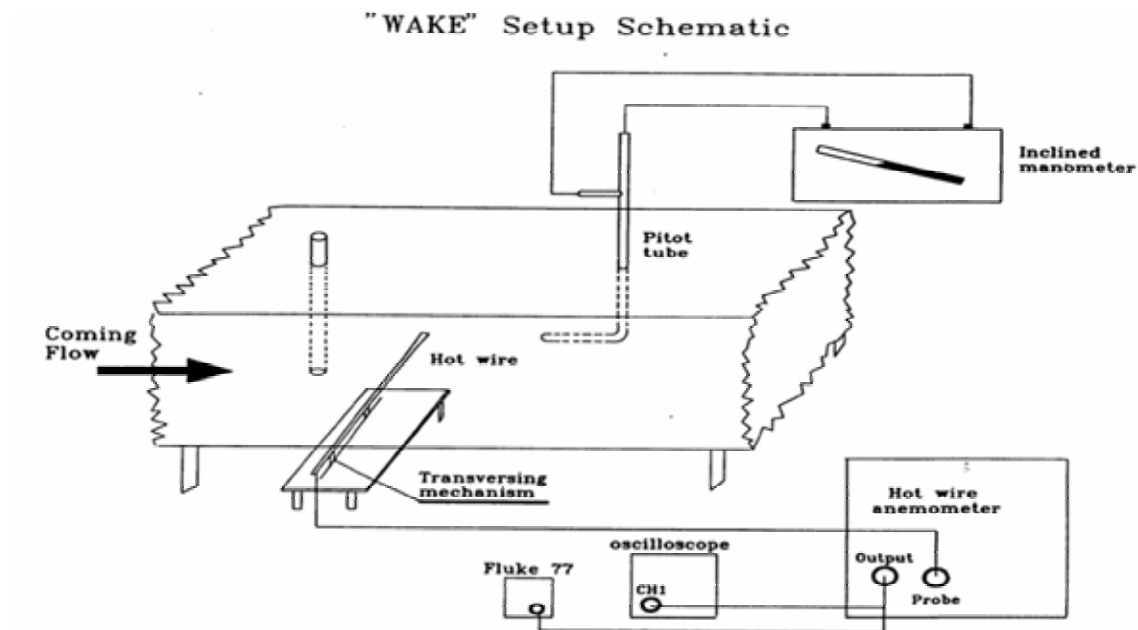


Figure 6: Wind tunnel and associated experimental setup.<sup>3</sup>

## 4.2 Anemometer Calibration

The first step before running any measurements with the hot wire is to do a calibration run. The internal resistance of the anemometer is set at 1.25 times the resistance of the hot wire probe's cold resistance which is measured with the Fluke 77. Before the tunnel is turned on, the manometer measurement of static pressure is noted. Manometer readings for Pt are taken for various tunnel velocities and the corresponding anemometer voltages are taken. This data will be used to fit a calibration curve, which will be used to determine all velocities measured hereon.

## 4.3 Velocity Profile Measurements

For all the steps in this experiment, the following steps were taken to measure the velocity profile downstream from an object. While running the tunnel at a given velocity, either the cylinder or airfoil is placed upstream from the hot wire. Starting the wire near the edge of the tunnel gives an indication of the free stream velocity. The hot wire is then moved towards the center of the tunnel until the velocity changes. Note that the anemometer voltage output is what is monitored as a function of the fluid velocity. Once the edge of the wake is found, back the hot wire up slightly so that data will start in the free stream. Measure the anemometer voltage and voltage rms on the oscilloscope noting the location of the hot wire probe by reading the micrometer on the transversing mechanism. The hot wire is moved at intervals across the wake noting the anemometer voltage and probe location at each point. When the wire passes all the way through the wake, the anemometer voltage will again reach the free stream value. This data can readily be converted in velocity profile information.

This procedure of velocity profile measurement was followed for the following cases (all TS numbers are in inches and refer to the diagram of the tunnel in the appendix figure 16):

1. The cylinder was kept at TS41 (6.75 in.) upstream and the velocity profile was measured at four different Reynolds numbers. We purposefully placed the cylinder close to the probe in order to facilitate easier measurements of the velocity wake at low tunnel speeds.
2. Keeping the tunnel at a medium velocity ( $R = 7 \cdot 10^3$ ) the cylinder was placed at three upstream distances from the hot wire: 6.75 in., 17.25 in., and 27.75 in.
3. Keeping the tunnel at a medium velocity ( $R = 7 \cdot 10^3$ ) the NACA 0010 airfoil at zero angle of attack was placed at the far upstream location TS22-26 (21.75 – 25.75 in. from the hot wire). The velocity deficits were too small the measure at this location within a good accuracy, so the airfoil was shifted up to TS36-40 (11.75 - 7.75 in. away).
4. The tunnel was kept at  $R = 7 \cdot 10^3$  and the airfoil was kept at the near distance TS36-40, while this time placed at a +3 degree angle of attack. Steps 2-4 were kept at the same tunnel speed for ease of comparison. The -3 degree angle of attack was not used since the airfoil is symmetric and the results would be the same.
5. Placing the cylinder at TS27 and 41, the oscilloscope was used to analyze the power spectrum of the fluctuating wake velocities. An attempt was made to find peaks in the power spectrum and correlate any frequencies as vortex shedding frequencies. The tunnel was turned up to maximum velocity, so as to easily get vortex shedding. The spectra were analyzed for several locations in the wake. These final measurements of vortex shedding frequencies were made in the last minutes that we had and consequently we were unable to obtain any substantial results.

## 5. Analysis of Results

### 5.1 Calibration

Fitting calibration data to King's Law (Eqn. 3) and using a least squares fit line gave the following calibration curves:

$\sqrt{U} = AV^2 + B$	Day One	Day Two
$y=U^{.5}; x=V^2$	$y = 0.6639x - 0.8055$	$y = 0.7192x - 0.8844$
$R^2$	0.9987	0.9973

Figure 7: Anemometer calibration results

#### Sample Calculation:

Ideal gas law:  $P = \rho RT$

Given ambient pressure (P), temperature (T), and the ideal gas constant (R=286); the density of air  $\rho =$

$$P/RT = (99335 \text{ Pa}) / (286 * 297.6 \text{ K}) = 1.167 \text{ kg/m}^3$$

Manometer reading:  $P_t = 1.317 \text{ in. H}_2\text{O} * (249.09 \text{ Pa/1 in. H}_2\text{O}) = 328.1 \text{ Pa}$

Anemometer output voltage: 2.048 V

Using Eqn. 2 with  $P_s = 319.6 \text{ Pa}$ :

$$U = [2 * (328.1 \text{ Pa} - 319.6 \text{ Pa}) / 1.1671 \text{ kg/m}^3]^{.5} = 3.810 \text{ m/s}$$

U is calculated from the various  $P_t$  measurements and then  $U^{.5}$  is plotted versus  $V^2$  according to Eqn. 3.

Microsoft Excel was used to fit the least squares line, which solves the system of equations ( $m=A$  and  $b=B$ ):<sup>1</sup>

$$\begin{aligned} m\left(\sum x_i\right) + nb &= \sum y_i \\ m\left(\sum x_i^2\right) + b\left(\sum x_i\right) &= \sum x_i y_i \end{aligned} \quad (12)$$

The  $R^2$  values indicate less than one percent error in the calibration of the anemometer.

## 5.2 Cylinder at TS41 for Various R

Figure 7 gives a picture of the velocity profiles for the cylinder at a distance of 6.75 in. With increasing Reynolds numbers the height of the curve increases due to the increase in the free stream velocity. Higher Reynolds numbers also show a steeper curve or velocity deficit in the wake resulting in a larger value of drag. Conversion of raw anemometer voltage data to fluid velocity was obtained through the use of the day one calibration yielding a smooth picture of the profile. Another thing seen in Fig. 7 is that the center of wake stay in the center of the tunnel (the wake stays symmetric).

### Sample Calculation:

Anemometer voltage reading at location .1016 m = 2.52 V

Using day one calibration:  $U = [.6639*(2.52^2) - .8055]^2 = 11.7 \text{ m/s}$

Dynamic Viscosity (Sutherland's Law):  $\mu = \mu_0 * [(T/T_0)^{3/2}] * [(T_0 + 198.6)/(T + 198.6)]$

$\mu = 3.74 * 10^{-7} * [(535.67 \text{ Rankin}/518.6 \text{ Rankin})^{3/2}] * [(518.6 \text{ R} + 198.6)/(535.67 + 198.6)] = 3.835 \text{ lb-s/ft}^2$   
 $= 1.836 * 10^{-5} \text{ kg/m*s}$

Kinematic Viscosity:  $\nu = \mu/\rho = (1.836 \text{ kg/m*s})/(1.167 \text{ kg/m}^3) = 1.57 * 10^{-5} \text{ m}^2/\text{s}$

Reynolds Number (Eqn. 4):  $R = U_\infty * d/\nu = (11.7 \text{ m/s} * .0127 \text{ m})/(1.57 * 10^{-5} \text{ m}^2/\text{s}) = 9400$

These U values correspond to u in Eqn. 7 and can be integrated using the trapezoidal method giving the drag, D. Eqn. 9 can then be rearranged to find Cd. Figure 8 gives a tabular result for the four Cd values found at TS41 and compares them to theoretically obtained values found through Eqn. 10.

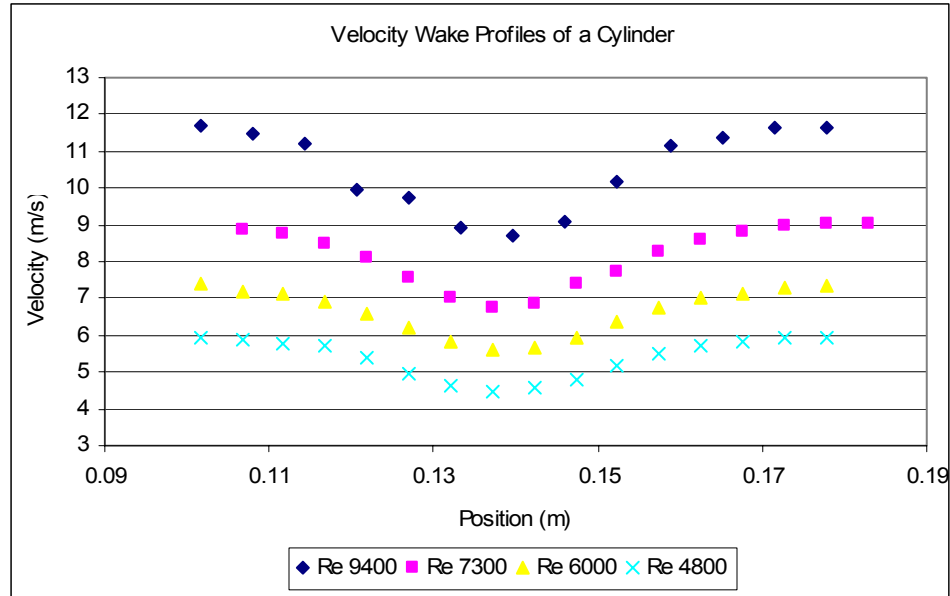


Figure 7: Velocity profiles for the cylinder at location TS41 (6.75 in. from the hot wire).

Reynolds Number	Experimental Cd	Theoretical Cd	Percent Error
9400	1.041 +- .027	1.022	2%
7300	1.038 +- .022	1.027	1%
6000	1.034 +- .026	1.030	<1%
4800	0.939 +- .024	1.035	-9%

Figure 8: Cd results for the cylinder at TS41

#### Sample Calculation:

Experimental Cd: Trapezoidal method of integration used for Eqn. 7.  $f(y) = u^*(U_\infty - u)$

For  $R = 9400$  at TS41,  $U_\infty = 11.7$  m/s.  $f(y)$  is computed at each location and then  $f(y)$  is integrated across the wake (only this area needs to be integrated since  $u$  goes to  $U_\infty$  outside of the wake). The trapezoidal method of integration is:

$$\int_a^b y dx \approx \sum_{i=1}^{n-1} \frac{1}{2} (x_{i+1} - x_i) (y_{i+1} + y_i) \quad (13)$$

For this sample calculation  $a = .1016$  m,  $b = .1778$ ,  $x$  is the position, and  $y$  is  $u^*(U_\infty - u)$  calculated at location  $x$ . The step size in  $x = x_{i+1} - x_i = .00635$  m.

The integral of  $f(y) = .5*(.00635)*[0 + 2(1.9 + 5.4 + 17.0 + 18.8 + 24.5 + 25.8 + 23.4 + 15.2 + 6.0 + 3.1 + .5) + 0] = .9 = D/(h*\rho)$  from Eqn. 7.

In Eqn. 10,  $A = h*d$ . Rearranging gives

$$Cd = 2*[D/(h*\rho)]*[1/(d*U_\infty^2)] = 2*(.9)*\{1/[(.0127m)*(11.7m/s)^2]\} = 1.041$$

$$\text{Theoretical Cd (Eqn. 10): } Cd = 1 + 10.0*R^{-(2/3)} = 1 + 10.0*(9400)^{-(2/3)} = 1.022$$

$$\text{Percentage Error} = [(Experimental Cd - Theoretical Cd)/(Theoretical Cd)]*100 = [(1.041 - 1.022)/(1.022)]*100 = 2\%$$

The only result experimental Cd result in agreement with theory is for  $R = 6000$ , although all are within 2% except for  $R = 4800$ . Perhaps we have underestimated the precision of our Cd measurement. It is logical to have worse results at low velocities because the velocity deficit is smaller and thus harder to measure. I might also note that the  $R = 4800$  measurement was the first one of the experiment, so there may be a significant amount of experimental error associated with that measurement. Contrastingly, at high velocities the amount of turbulence is higher in the wake contributing to an imprecision in measuring the velocity. This is why our mid-range data seems to fit best. The imprecision experimental Cd stems from computational error of the trapezoidal rule, velocity fluctuations due to turbulence, and a level of ambiguity associated with selecting  $U_\infty$ . The trapezoidal rule error is order  $(1/N^2)$  for N number of intervals. We have used this as a rough error estimate for the integration and have propagated it through the experimental Cd calculation. It can be observed in the wake profiles in Fig. 7 that the velocity measurements at the both sides of the wake are not exactly equivalent, thus resulting in an error in selecting the free stream velocity.

#### Sample Calculation:

$$\text{Error in } U_\infty: \Delta U_\infty = U_\infty * [(4*\Delta V)/V] = 11.7 \text{ m/s} * [(4*.005 \text{ V})/2.522 \text{ V}] = .1 \text{ m/s}$$

$$\text{Error in trapezoidal rule: } \Delta [D/(h*\rho)] \approx 1/N^2 = (1/11^2) = .008$$

$$\Delta(Cd) \approx Cd*[2*(\Delta U_\infty/U_\infty) + \{\Delta [D/(h*\rho)]/[D/(h*\rho)]\}] = 1.041*[(2*.1\text{m/s})/11.7 \text{ m/s} + (.008/.9)] = .027$$

### 5.3 Cylinder at Various Downstream Positions for $R = 7000$

Three velocity profiles were measured for positions at TS41, 30.5, and 20 (6.75 in., 17.25 in., and 27.75 in. from the hot wire). The velocities  $u$  in the wakes were computed using the same method as above. Closer to the cylinder (TS41) the profile is thin and the deficit is large (Fig.8). As the wake travels downstream it broadens while at the same time keeping the same geometry and the same drag (related to the integral of the velocity deficit by Eqn. 8). This confirms the theoretical picture of a cylinder wake spreading downstream presented in Fig. 4. Also from Fig.8 it is noted that since the curves are all centered around the same location, the wake travels straight downstream.

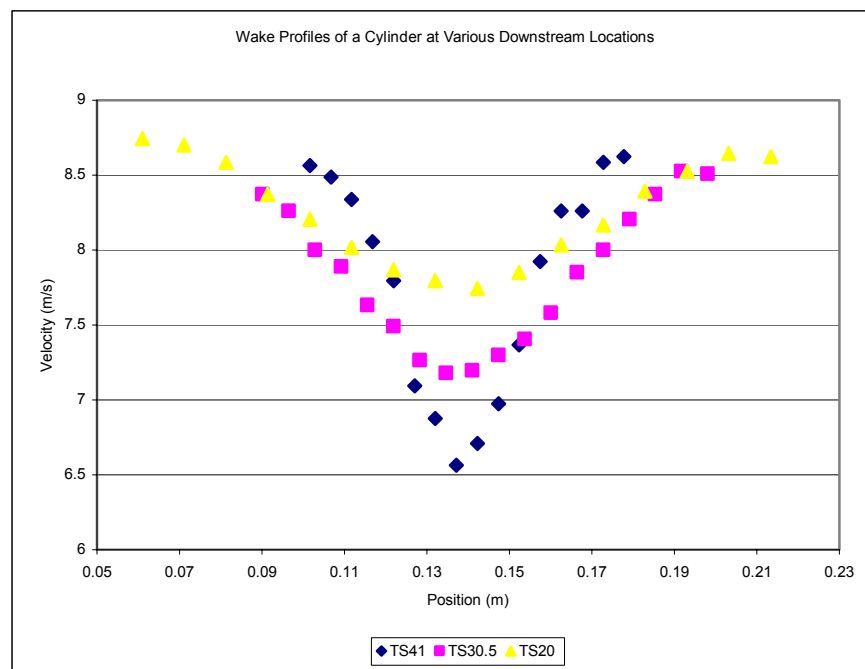


*Figure 8: Wake Profiles of a Cylinder at Various Downstream Locations for  $R=7000$*

Eqn. 6 takes the velocities  $u$  and puts them in terms of the velocity deficit  $u_1$  and Eqn. 11 gives a relation for analyzing the self-similarity of the profiles by normalizing the width and height of the profiles. Experimental results along with the theoretical curve are given in Fig. 9.

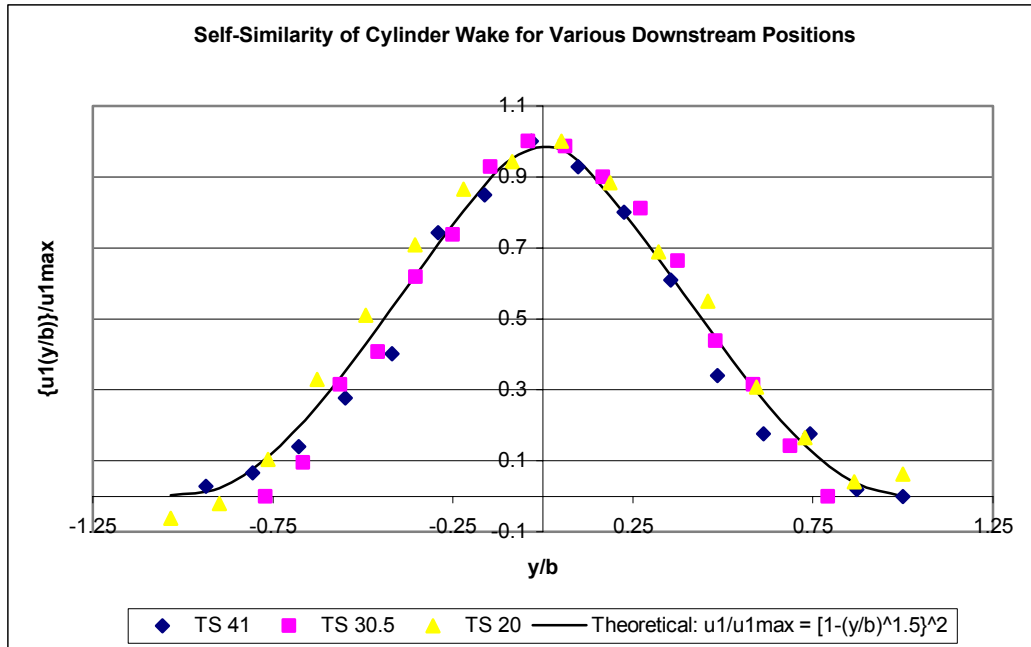


Figure 9: *Self-Similarity of Cylinder Wake for Various Downstream Positions at  $R = 700$*

**Sample Calculation:**

At TS41: velocity  $u = 8.5$  m/s at location  $y = .10668$  m

(this is the second diamond point from the left in Fig. 9)

$b = .03937$  m,  $U_\infty = 8.6$  m/s,  $y_0$  (middle of the tunnel) =  $.13843$  m

$u_1 = U_\infty - u = 8.6$  m/s  $- 8.5$  m/s =  $.1$  m/s      (after all  $u_1$  calculated find  $u_{1max} = 2.06152$  m)

$u_1/u_{1max} = (.1\text{m/s})/(2.06152\text{m}) = .07$

$y/b = (.10668\text{ m} - .13843\text{m})/.03937\text{ m} = -.80645$

The plot in Fig. 9 indicates that we were able to confirm the theoretical self-similar relation given in Eqn. 11. The experimental values vary just slightly even as you continue downstream. As in Sec. 5.2, the velocity profile can be used for measuring  $C_d$ .

Distance from Hot Wire (in.)	Experimental Cd	Theoretical Cd	Percent Error
6.75	1.041 +- .024	1.027	1%
17.25	1.038 +- .023	1.028	1%
27.75	1.129 +- .026	1.027	10%

*Figure 10: Cd at Various Distances from the Cylinder at R = 7000*

The closer measurements are in agreement with the theoretical values, but the farthest measurement does not since the accuracy of measuring the velocity profile of the wake goes down as you move away from the cylinder. As shown in Fig. 8 as the wake moves downstream, the velocity profile broadens and the velocity deficit decreases. When further downstream the hot wire must traverse a larger distance and the velocity values are harder to measure causing the absolute error increases. This problem of measuring a small velocity deficit was the same as encountered in measuring the wake a low Reynolds numbers in Sec. 5.2.

#### **5.4 Drag on a NACA 0010 Airfoil**

As described in the procedure, the NACA 0010 airfoil wake was observed at the same free stream velocity (8.4 m/s) as the cylinder though this results in a higher Reynolds number ( $R = 55700$ ) since the chord length is 4 in. and not the  $\frac{1}{2}$  in. diameter of the cylinder. First the airfoil was placed farther away from the hot wire, but this resulted in small variations of the velocity for the velocity deficit (as noted for the cylinder, if the downstream distance is too far the data is off significantly). This velocity profile is uneven and not useful, but can be observed in the appendix. Moving the airfoil closer to the hot wire (7.75 in. from the trailing edge) produced very good results. Fig. 11 plots the velocity profile of the airfoil at this location for both 0 and +3 degrees angle of attack.

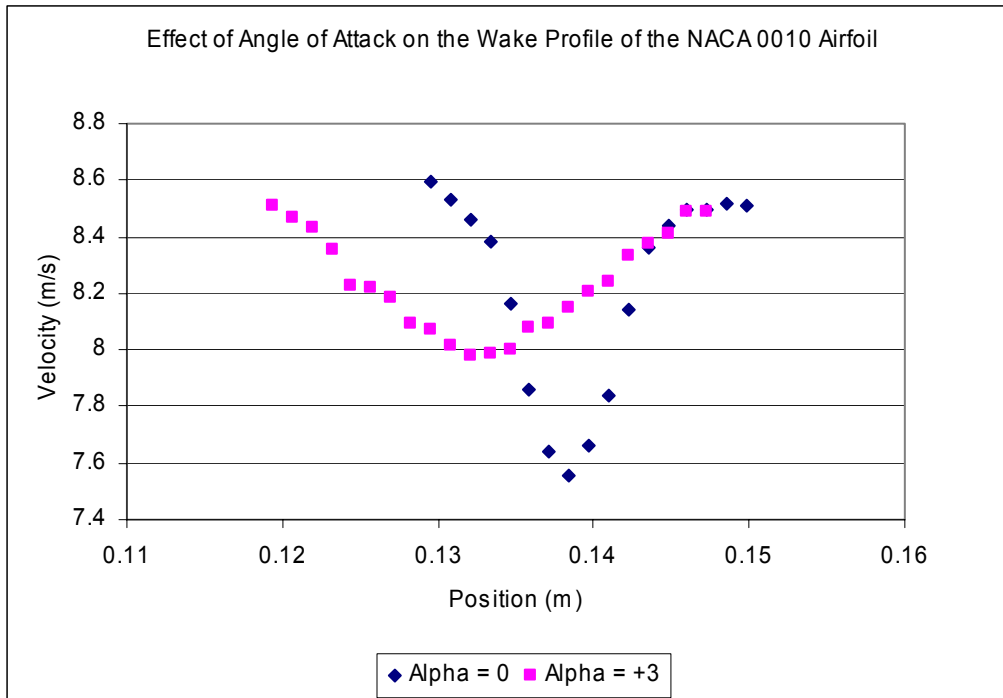


Figure 11: Velocity Profile for the Airfoil Trailing Edge 7.75 in. from the Hot Wire with the Airfoil at 0 and +3 degrees Angle of Attack.

Zero angle of attack results in a thinner wake with a higher  $u_{1max}$ , while at +3 degrees angle of attack the velocity profile is shifted over and broadened. Although the zero angle of attack profile has a larger maximum deficit, the profile at an angle of attack produces more drag as indicated in Fig. 12.

Angle of Attack (deg)	Experimental CD	Theoretical CD (found using Xfoil)	Percent Error
0	0.0154 +- .0014	0.0166 +- .007	-7%
3	0.0178 +- .0007	0.0195 +- .007	-9%

Figure 12: Experimental and Theoretical Results for Airfoil at  $R = 55700$  and 7.75 in. to the Trailing Edge.

The experimental Cd result at zero angle of attack is in agreement with the theoretical and the +3 degree result is quite close. The larger percent error is again due to the fact

that the velocity deficit being measured is quite small compared to the fluctuations. If we were to repeat this lab, we would measure the airfoil drag at the maximum tunnel speed. Comparing to the cylinder, the drag is reduced considerable. Also, the percentage error is greater for the +3 degrees angle of attack because the wake is wider and the deficit shallower than at 0 angle of attack. Looking through literature, we could not find a comparable experiment at this Reynolds number, so we did a numerical simulation using Xfoil. The error for the Xfoil is roughly taken from the  $C_l$  at zero angle of attack (-.0067), which should be zero. Both Xfoil runs for the NACA 0010 at 0 and +3 degrees are placed in the appendix.

### 5.5 RMS Fluctuations

For all the velocity profile measurements, data was taken for the fluctuations ( $V'$ ) in the mean voltage ( $V$ ). This gives a measure of how much the velocity is fluctuating and the turbulence levels in the wake. Measuring these fluctuations across the wake presents a picture of how turbulence is ordered in the wake. Assuming small fluctuations, voltage fluctuations can be converted into velocity fluctuations ( $U'$ ).<sup>3</sup>

$$U' \approx 4(A\bar{V}^2 + B)A\bar{V}V' \quad (14)$$

#### Sample Calculations:

Cylinder at TS41 and  $R = 7000$

At location  $y = .1016\text{m}$ ,  $V = 2.302\text{ V}$ ,  $V' = .022\text{ V}$ , Calibration Day Two:  $A = .7192$  and  $B = -.8844$

Using Eqn. 14:  $U' = 4[.7192(2.302)^2 - .8844]*.7192*2.302*.022 = .43\text{ m/s}$

The velocity fluctuations for the cylinder wake at TS41 and  $R = 7000$  are plotted along with the velocity profile in Fig. 13. The RMS fluctuation scale is on the right side, while the left side has the mean velocity scale. The fluctuations increase as you go into the wake and reach a maximum at the middle of the wake. The turbulence is in the middle of the wake and dies out as you go farther from the center.

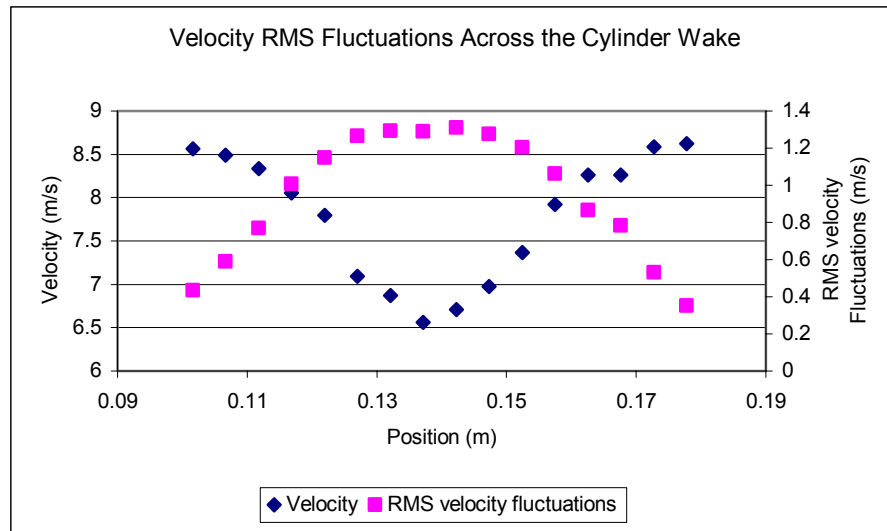


Figure 13:  $V_{rms}$  Fluctuations for the Cylinder at TS41 and  $R = 7000$ .

Using Eqn. 14, the fluctuations for the airfoil at zero angle of attack, a distance of 7.75 in. from the trailing edge to the hot wire, and  $R = 55700$  are plotted in Fig. 14 against the mean velocity profile. In this case the fluctuations are not as large as the cylinder's. The fluctuations follow the same trend as for the cylinder (increasing when approaching the center of the wake from the free stream) except for a decrease at the very center of the wake. This can be seen as an effect seen in Fig. 3D. Turbulence is spinning off two trailing vortices, while a streamline runs down the center of the wake. Thus, at the very center of the wake, the fluctuations are diminishing while they increase in pairs of vortices about the centerline.

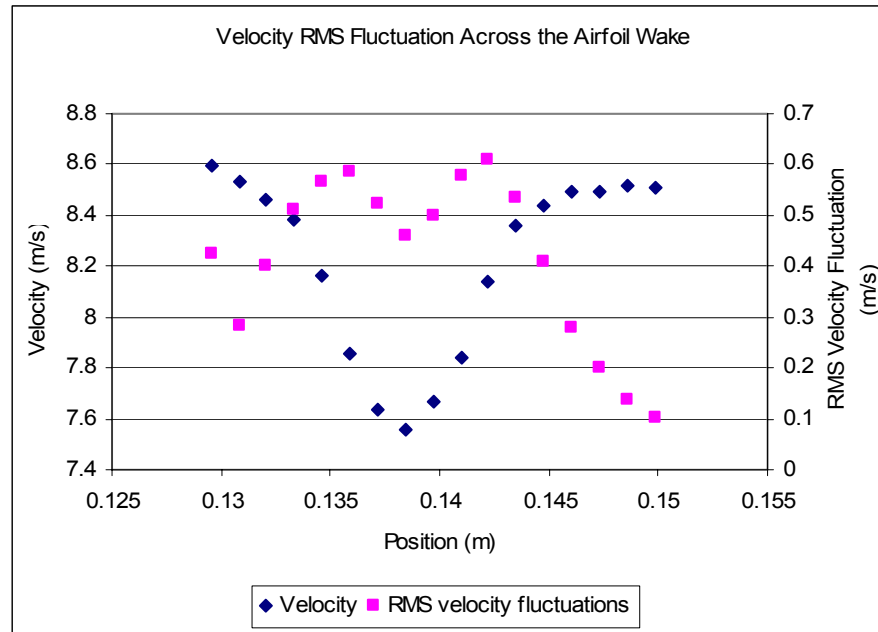


Figure 14:  $V_{rms}$  Fluctuations for the Airfoil at Zero Angle,  $R = 55700$ , and at a Distance of 7.75 in. to the Trailing Edge.

## 6. Discussion

### 6.1 Tunnel Effects 2-D

There will always be problems with taking experimental data, as the mechanism will always cause an intrusion on the ideal test conditions. If the wind tunnel is considered as the testing region, then added to the use of measuring probes are the walled boundaries of the test section. While this feature may not be prevalent for many wind tunnel tests, in the case of aircraft testing this region should be as close to ‘free air’ as possible. This can be achieved by ensuring the ratio between the size of the tunnel to the size of the body being analysed is large. In practice however the use of infinitely spanning tunnels, or minute test sections are either too expensive, or do not provide a reasonably accurate result.

One major feature of tunnel scale effect was that of the walls affecting the wake profile. That is to say, not the boundary layer interaction, but the region of air that lies between the ‘edge’ of the wake profile and the tunnel wall. While the relative size of the body with respect to the tunnel dimensions was small, it must be noted that the wake extended much further from the body than the diameter of cylinder, or the profile thickness of the Airfoil. As the wake contains flow that has lower velocity than the surrounding flow, according to Bernoulli’s principle for an Ideal fluid, the flow region around the wake must accelerate to a higher velocity in order to satisfy the continuity equation. While air is far from being an Ideal fluid, it is safe to assume that at such a low Reynolds number the effects of compressibility will not have a great effect.

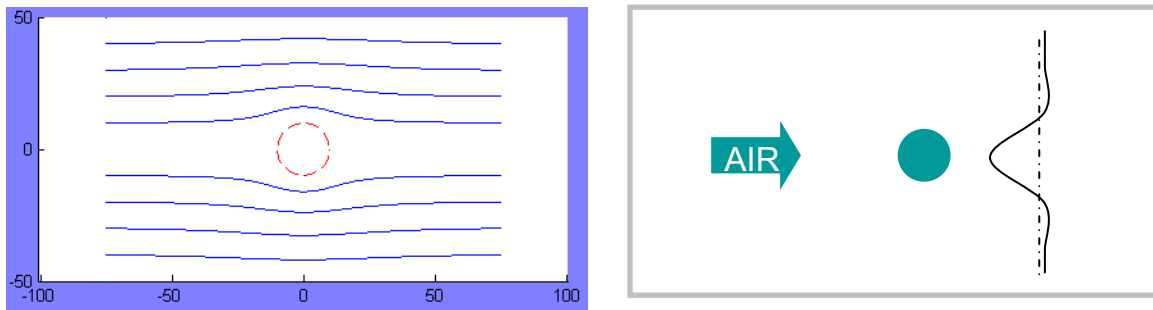


*Figure 15a: (Left) Streamlines produced around a cylinder using a Potential function (doublet+ freestream). Figure 15b. (Right) schematic of the velocity distribution behind a cylinder in a test section*

We can analyse the effect of a bluff body in a flow field by using potential flow, shown in Figure 15a. The effect of combining a uniform flow field with a doublet causes streamlines to separate from the central flow region. Coupled with the restriction of the walls on either side must cause the flow to increase in velocity. The downstream effect of this phenomenon is shown in figure 15b , where the solid line represents a standard velocity profile taken from our results, and the dashed line represents the velocity profile if there were no cylinder upstream. The question that therefore still remains is where to take the value for the freestream velocity measurement in order to provide the baseline for the drag integration.

During the investigation a lot of care was taken with the initial freestream measurement. As this was the potential source of the greatest error in the drag calculation. The freestream measurement was taken far out of the downstream wake of the cylinder towards the wall where a reasonably accurate result could be obtained.

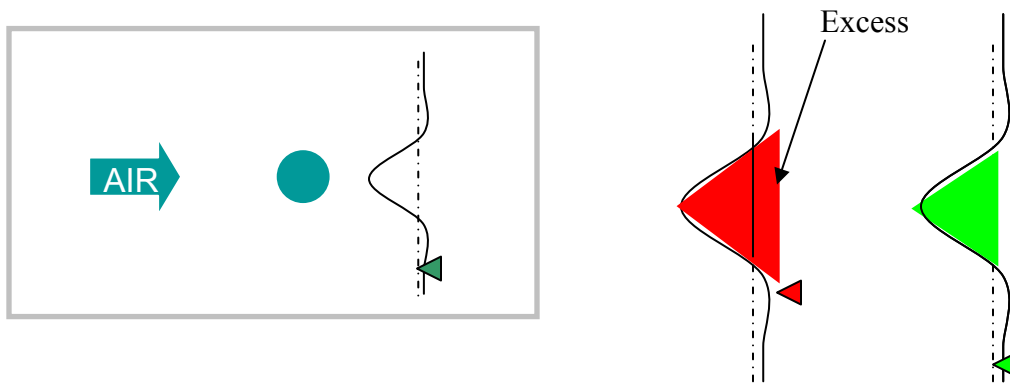


*Figure 16: Location of freestream velocity measurement in order to gain more accurate results.*

It was hoped that by taking a measurement of the freestream at this location the excess portion of the wake profile, shown in figure 16 would not be measured, which would give a better estimate of the drag. However, since the freestream was measured while the cylinder was in the tunnel, this would account for the general trend in our results giving higher estimations of drag than previously measured empirical data, or CFD data. There was still also a great deal of ambiguity of where to take this freestream value.

## 6.2 Vortex Shedding Frequencies

After a short investigation into the vortex shedding behaviour of the cylinder it was clear from the oscilloscope readings that no frequencies that would reasonably be caused by a set of shedding vortices could be found. Two locations were used in the investigation, where the data from the TS27 location has been included in the appendix. Using both the fast Fourier transform function provided by the Lecroy oscilloscope, and a further

averaged FFT from the captured data, only peaks at much higher frequencies could be found. These plots have been included in the appendix, but no supportable conclusions can be gained from them.

## 7. Conclusions

Anemometer calibrations followed theoretical expectations from King's Law (Eqn. 3) and were quite accurate with  $R^2$  values around .998 giving A and B with little to no error. A majority of our  $C_d$  measurements for both the cylinder and airfoil were in agreement with theoretical results given the precision of the experiment. Those results that were not in agreement were cases where the velocity deficit was too small and difficult to measure. These cases occurred at large downstream distances and low free stream velocity levels. A majority of the  $C_d$  results were within 1 or 2% error, which is quite appreciable. Only two cases had errors larger than this: the cylinder at  $R = 4800$  and at 27.75 in. distance downstream. Qualitatively, we observed the cylinder wake broaden while the velocity deficit decreased as the downstream location was increased. The Eqn. 11 self-similarity relation for wake profiles was confirmed for three locations downstream from the cylinder. These results turned out particularly nicely.

The zero angle airfoil drag measurement was in agreements with our computational measurement using Xfoil. The  $C_d$  result for +3 degrees was not in agreements, but was very close. Percentage errors in airfoil drag were quite larger than cylinder (~8% compared to 2%) and this was due to the difficulty in measuring the smaller velocity deficits. The airfoil geometry is quite advantageous as it results in 1% of the drag created by the cylinder. Fig. 11 shows that the effect of the angle of attack is to clearly shift the wake, broaden it, which results in a larger  $C_d$ . Since the tunnel and airfoil are symmetrical, we did not perform the experiment at -3 degrees since it should give the same result.

Another indication of what is going on in the wake is Figs. 13 and 14, which show the velocity fluctuations while crossing the wake. The cylinder had turbulence levels high at the center the wake and trailing off when approaching the outer edges. The airfoil fluctuations follow the same pattern, but with a dip in the center of the wake associated with a calm streamline down the center as seen in Fig. 3D.

The majority of error in this lab is due to fact that the velocity levels are turbulent and fluctuating. This creates an inherent precision error in all velocity measurements. Other lower factor errors are due to error when performing the trapezoid method of integration. This could be reduced by taking more intervals or using a different, more accurate method of integration. Another error is due to a level of ambiguity when deciding the free stream velocity. In many runs the free stream is smaller on far side of the tunnel. This could be due to the fact that the hot wire is traversing across the wake and interacting with the wake velocities. To correct for this, maybe we should have taken a run across the tunnel at several velocities without any object in the tunnel. This would give an indication to the level of uniformity in the free stream velocity and correct for interactions between our measure instrument (the hot wire and traversing mechanism) and the fluid flow. All in all, this lab made it quite easy to visualize what occurs in a wake behind an object and allowed for fairly accurate measurements of  $C_d$ , which were mostly within 2% of theoretical values.

## 8. References

1. "Background Information for Use of Pitot Tube, Manometer, Hot Wires, and Hot Films." AAE520. Purdue University. 2004.
2. Currie, I.G. *Fundamental Mechanics of Fluids*, 3<sup>rd</sup> ed, Marcel Dekker, Inc., New York, 2003.
3. "Hot Wires, Wakes, and Drag Measurement." AAE520. Purdue University. 2004.

- Xfoil 6.94 executable for Win32, optimized for Pentium 4.  
<http://raphael.mit.edu/xfoil/>

## 9. Appendix

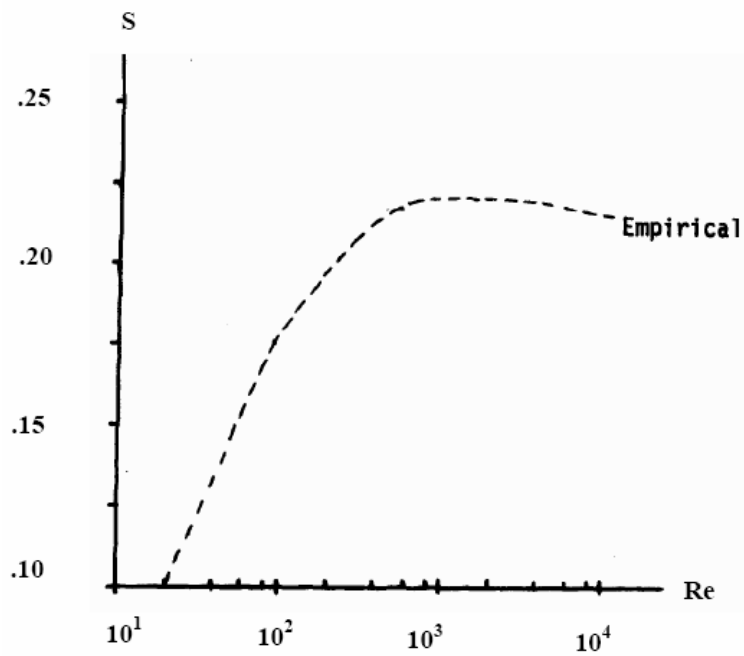


Figure 17: Empirical Correlation between Strouhal Number and Reynolds Number.

### Modifications to Wake Tunnel for AAE520

S.P. Schneider, 12 Feb. 2003.  
 Add additional part for airfoil positioning  
 to allow measurement in two aft locations.  
 Add additional holes for cylinder.

Top view of plexiglas test section. Schematic.  
 Test Section (TS) stations measured from  
 upstream end of plexiglas.

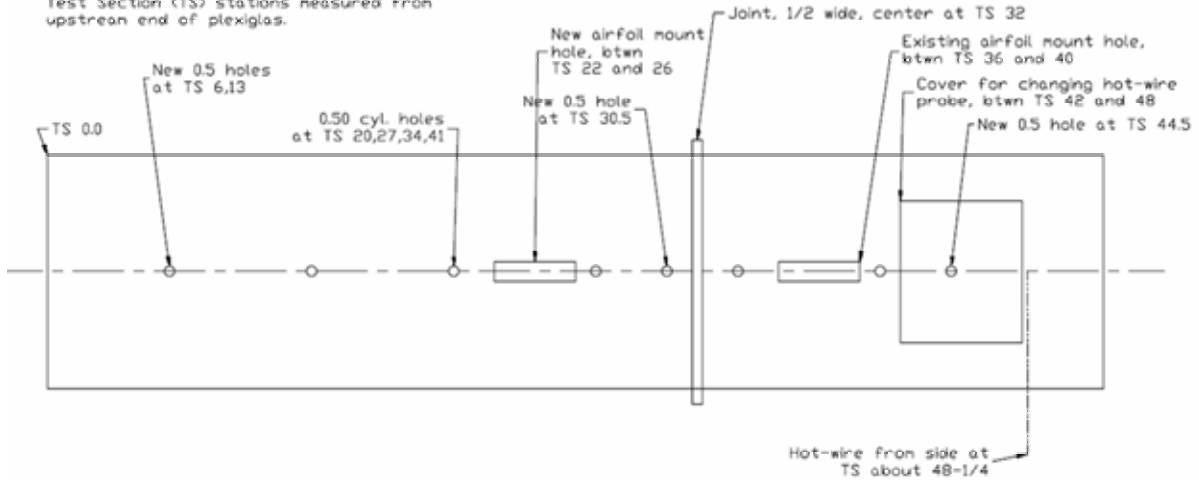


Figure 18: Diagram of Wake Tunnel and Various Test Section Positions

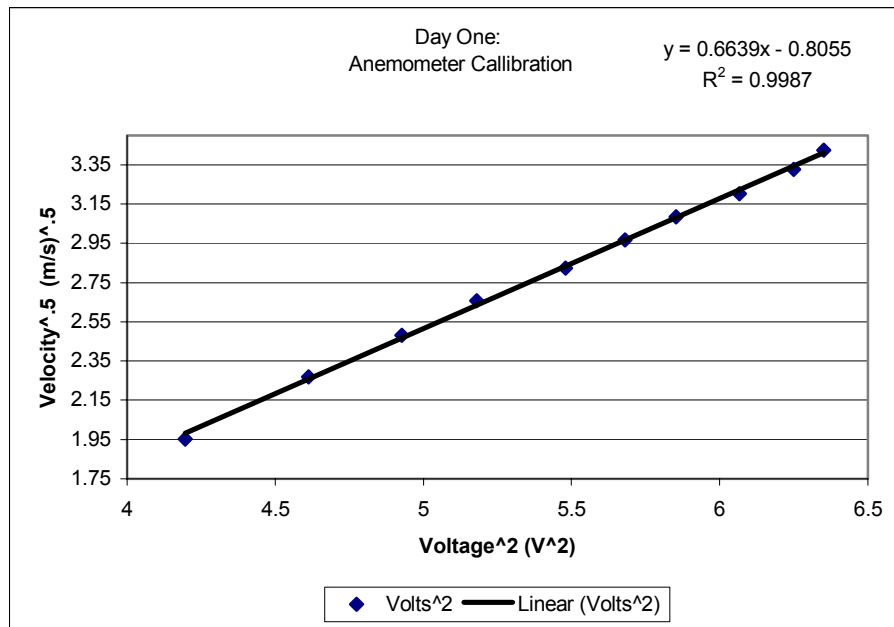


Figure 19: Anemometer Calibration for Day One

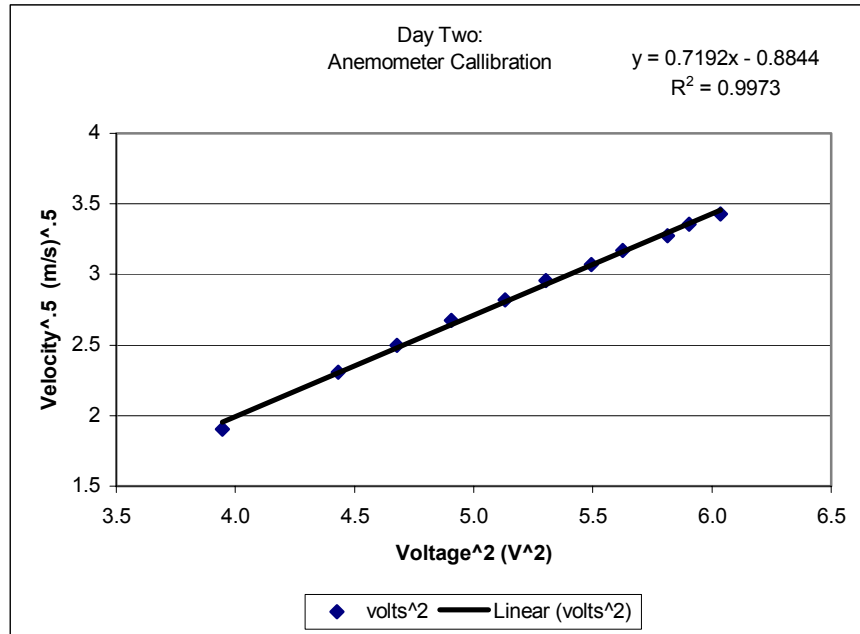


Figure 20: Anemometer Calibration for Day Two

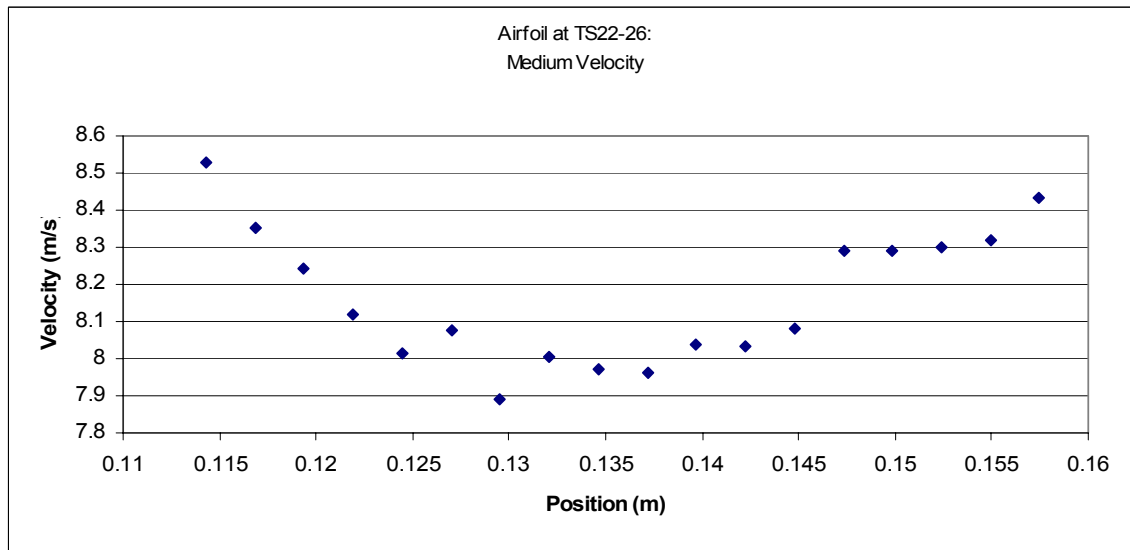


Figure 21: Airfoil at  $R = 55700$ , Zero Angle, and at Far Location

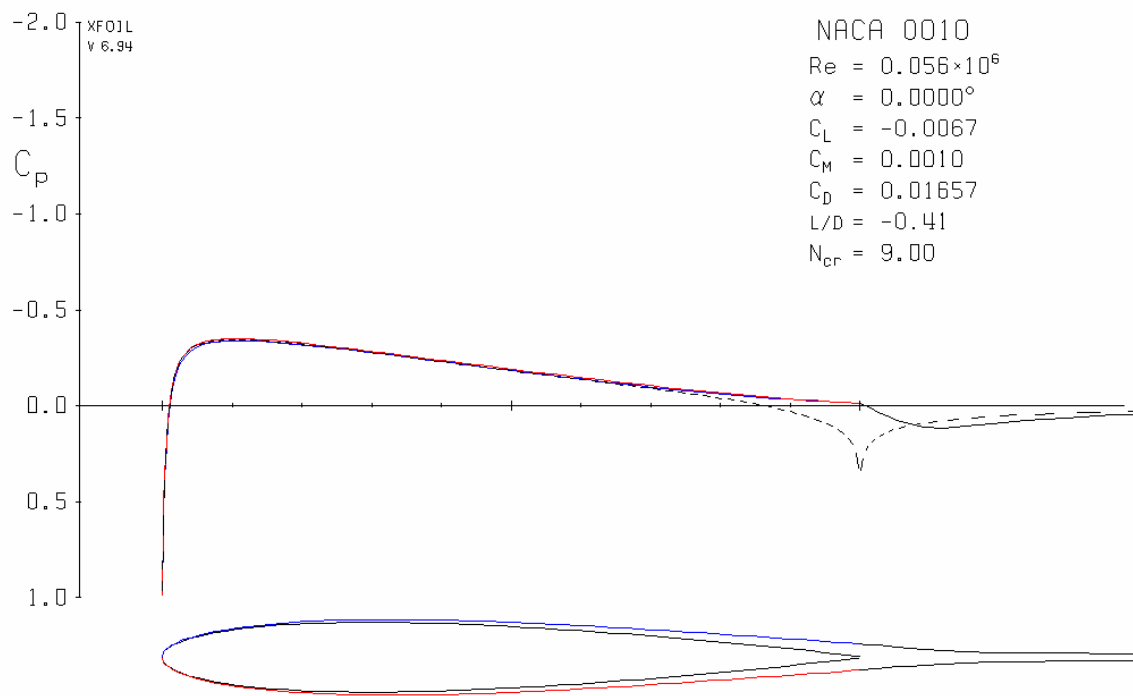


Figure 22: Xfoil Run Simulation of NACA 0010 at Zero Angle of Attack.

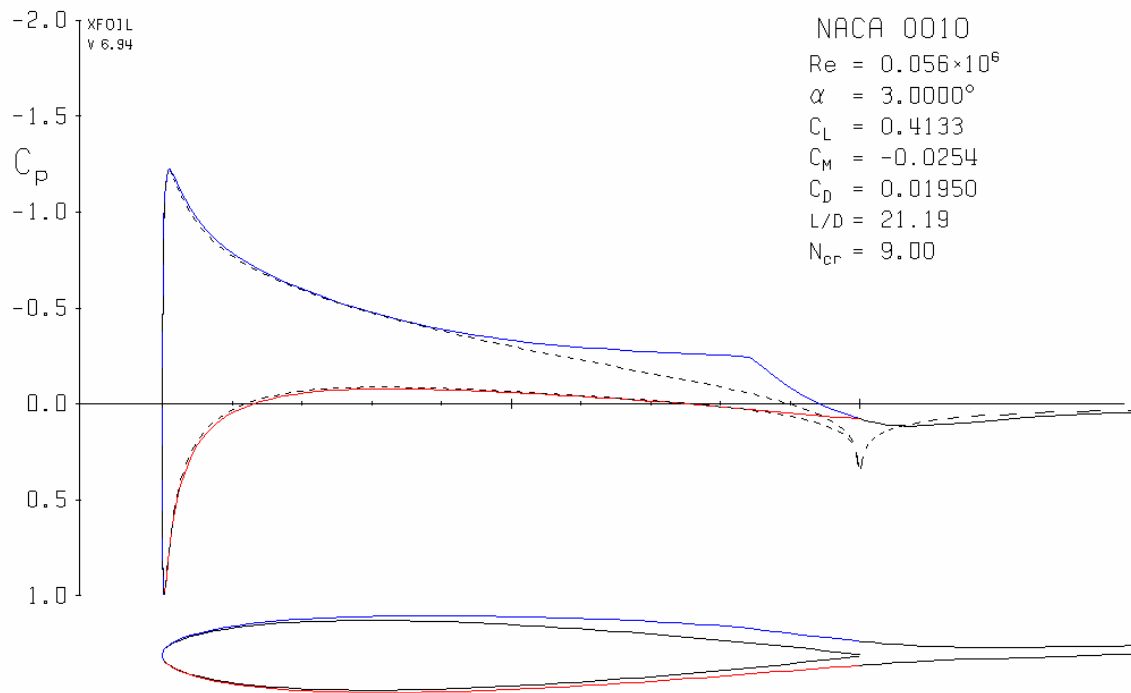


Figure 23: Xfoil Run Simulation of NACA 0010 at +3 Degrees Angle of Attack.

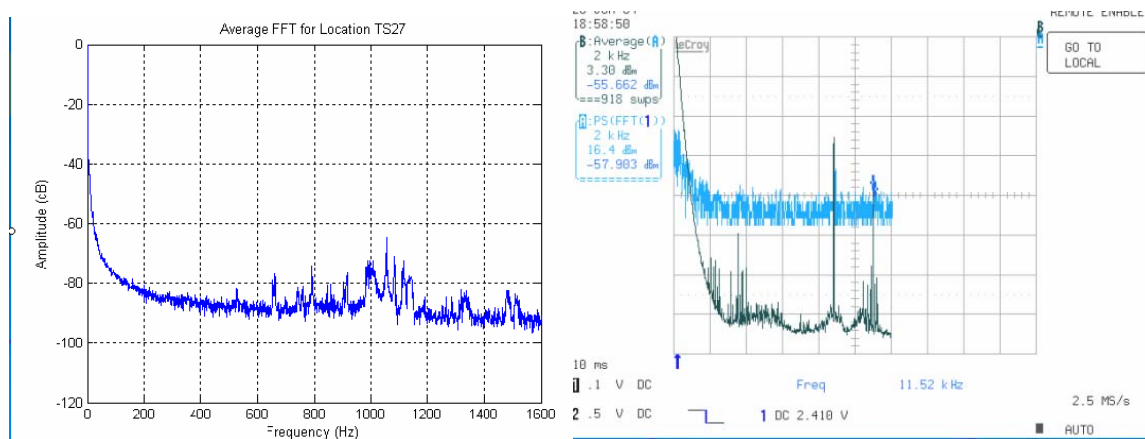


Figure 24a: Average FFT for location TS27 using MATLAB. Figure 24b: An FFT plot and an Average FFT plot using the Lecroy oscilloscope at location TS27